*J Mater Sci* (2017) 52:4608–4620

# Evaluation of morphology and photoluminescent properties of $PbMoO_4$ crystals by ultrasonic amplitude

G. M. Gurgel[1], L. X. Lovisa[1,*], O. L. A. Conceição[1], M. S. Li[2], E. Longo[3], C. A. Paskocimas[1], F. V. Motta[1], and M. R. D. Bomio[1,*]

[1] *Department of Materials Engineering, Federal University of Rio Grande do Norte, Campus Lagoa Nova, Natal, RN CEP 59072-970, Brazil*

[2] *IFSC, USP, Av. Trabalhador São Carlense, 400, São Carlos, SP CEP 13566-590, Brazil*

[3] *LIEC, IQ, UNESP, Rua Francisco Degni s/n, Araraquara, SP CEP 14801-907, Brazil*

**Received:** 28 August 2016
**Accepted:** 20 December 2016
**Published online:** 30 December 2016



## ABSTRACT

Lead molybdate ($PbMoO_4$) crystals were synthesized by the facile sonochemical method at 20 kHz frequency with a variable ultrasonic amplitude and synthesis time. These crystals were structurally characterized by X-ray diffraction (XRD). Field emission scanning electron microscopy images were employed to observe the evolution of the crystal growth process. XRD patterns indicate that these crystals have a scheelite-type tetragonal structure. The growth mechanism of $PbMoO_4$ crystal was proposed to explain the development stages starting with precipitates formed by particles with disordered growth to form dendritic structures. The effect of the amplitude processing applied was rather significant for the size range of the particles produced. The optical properties were analyzed by ultraviolet–Visible (UV–Vis) absorption spectroscopy and photoluminescence (PL) measurements. The spectrum shows that the sample has a typical green emission. The origin of the PL emission spectrum of the metal molybdates might be ascribed to the charge-transfer transitions within $[MoO_4]$ clusters.

## Introduction

Molybdate metal materials are widely studied because they have important optical, electronic, and magnetic properties. Thus, they have attracted great attention because of their applications in photoluminescence, in catalysis, in scintillator materials, and humidity sensors [1–3]. Among the metal molybdates, the $PbMoO_4$ shows a structure of the a scheelite-type tetragonal structure with a *4/m* point group symmetry and an *I41/a* space group, with two formula units per primitive cell [4, 5]; in these systems, the Mo atom is coordinated by four O atoms, forming a tetrahedral configuration $[MoO_4]^{2-}$, and Pb atom is coordinated by eight adjacent O atoms forming the configuration $[PbO_8]^{2-}$. $PbMoO_4$ has

O. L. A. Conceição *In memoriam*.

Address correspondence to E-mail: lauraengmat@hotmail.com; mauricio.bomio@ct.ufrn.br



DOI 10.1007/s10853-016-0705-y

been synthesized by several chemical methods such as solvothermal, Czochralski crystal growth, and hydrothermal microwave [6–8]. Despite the success in getting the $PbMoO_4$, some of the factors limiting the application of the Czochralski method are the level of complexity in the experimental procedure and the conditions of synthesis are very restricted. The $PbMoO_4$ microcrystals produced from traditional chemical routes exhibit a variable morphology and large crystal size. These characteristics are related to the rapid growth of the crystals.

During the growth of $PbMoO_4$ crystals, crystal facets that have high surface energy have a strong fall of this energy. As for $PbMoO_4$, a crystal growth along [001] crystal direction is preferred to the [100] direction because the average surface energy of (001) facets is higher than the (100) facets [9]. The growth of crystals through the direction [001] can produce $PbMoO_4$ microcrystals with octahedron-like morphology with small facets (001) exposed at the top and bottom of the octahedron-like microcrystals. Dong and Wu [10] demonstrated the growth mechanism of the $PbMoO_4$ crystal from the liquid membrane system supported vertically. It was observed that crystal growth had already been reported in the literature known as oriented attachment [11]. Such growth is characterized by self-assembled adjacent particles; these particles display the same crystallographic orientation. The crystals can also present a growth based on Ostwald ripening mechanism [12]. In this case, the larger crystals grow at the expense of smaller crystals. This crystal growth occurs by addition atom by atom, where there is dissolution of a unstable phase and reprecipitation of a more stable phase. This is a spontaneous process, as the larger crystals are thermodynamically more stable as compared with smaller crystals.

The nucleation and growth are the two stages proposed for the study for the formation and growth of crystals [13]. Cavalcante [14] shows that the morphology and size of crystals are a function of the average solution concentration, classified as unsaturated, saturated, and supersaturated. The nucleation step occurs when precipitation occurs from a saturated solution. The nuclei acquire stability and are able to overcome the energy barrier from the increased concentration of the solution (supersaturated). Secondly, these nuclei are grouped starting from the stage of growth of the crystals [15]. Increased attention has been paid to the controlling of the morphology and size of particles obtained by chemical methods because these characteristics can affect its properties and performance compromise their technological applications.

The ceramic class of molybdates has attracted interest in several scientific and technological areas due to its numerous applications in the industrial area, including scintillation detectors, optical fibers, humidity sensors, solid state lasers, catalysts, and photoluminescent devices [16–18]. Studies have been intensified in order to obtain new functionalities and behaviors with respect to their wide extension of properties and applications [19]. In particular, recent theoretical and experimental studies on the optical properties of lead molybdate ($PbMoO_4$) have been reported in the literature [20, 21].

In order to improve the preparation of $PbMoO_4$ monocrystals, Sabharwal [22] with previous knowledge of the synthesis parameters, such as direction of growth of the monocrystal, temperature gradient that may affect its growth, also observed that deviations in stoichiometry of $Pb^{2+}$ ions of the material influence the optical properties and cause stretches in the crystalline structure causing cracks in the monocrystal. In addition, these researchers found that due to these small variations in the stoichiometry of the material observed, the photoluminescence property in the bands of the green and blue spectrum of the monocrystal could be observed at room temperature.

The use of ultrasonic radiation to produce materials has been widely applied [23, 24]. Unlike other methods, the sonochemical method requires only the presence of a liquid medium to produce their effects. The ultrasound irradiation in the liquid promotes the important phenomenon known as cavitation. This phenomenon provides sufficient conditions for the chemical reaction to occur. The steps belonging to cavitation are formation, growth, and implosion of bubbles in a liquid [25].

This study was to evaluate the effect of ultrasonic radiation on the morphology of $PbMoO_4$ crystals and their photoluminescent properties. Growth mechanism of the crystals, as well as the influence of the synthesis time and amplitude applied to the process, has been proposed.

## Experiment procedure

### Co-precipitation and sonochemical synthesis of $PbMoO_4$ crystals

The $PbMoO_4$ particles were synthesized by sonochemical method [26] at 20 kHz frequency, using the molybdic acid (Alfa Aesar, 85%) and lead nitrate (Aldrich, 99%) as precursors without any surfactant.

The typical synthesis procedure is described as follows: In a beaker, $5.0 \times 10^{-3}$ mol of molybdic acid ($H_2MoO_4$) was dissolved in 50 ml deionized water. Then the lead nitrate ($5.0 \times 10^{-3}$ mol) was added to the solution. The pH of the solution was adjusted to 9 by adding ammonium hydroxide ($NH_4OH$) (Synth, 30% $NH_3$) to it, observing the formation of the a white precipitate (co-precipitation method). The resulting solution was exposed to high-intensity ultrasonic irradiation (Branson Digital Sonifier) in a continuous mode with three different amplitudes 65, 75, and 85% and two times 30 and 45 min duration of the synthesis (sonochemical method).

Then the result powders were separated from the solution by centrifugation at 10,000 rpm and washed four times with deionized water to remove any ammonium hydroxide residual molecules. The powders were dried in a furnace at 80 °C during 12 h.

### Characterization of $PbMoO_4$ Crystals

The phases present in the ceramic powder were investigated by X-ray diffraction (XRD) using the diffractometer Shimadzu XRD-7000 model with CuKα radiation ($\lambda = 1.5406$ Å) in the range $2\theta$ of 10°–75° (5°/min). The distribution of particle size and morphology were investigated by Supra 35 VP-FEG-SEM (Carl Zeiss, Germany) operated at 6 kV. The UV–Vis reflectance spectra of the $PbMoO_4$ particles were measured using Cary equipment, model 5G, in the 200–800 nm range. Photoluminescence spectra were obtained using a Thermal Jarrell-Ash Monospec 27 monochromator and Hamamatsu R446 photomultiplier. The excitation source used on the samples was a laser at a wavelength of 350 nm with krypton ions (Coherent Innova) with an output of approximately 13.3 mW; all measurements were performed at room temperature.

## Results and discussion

### XRD pattern analyses

XRD patterns of $PbMO_4$ synthesized by sonochemical method are shown in Fig. 1. XRD patterns revealed that all diffraction peaks of $PbMoO_4$ can be indexed to the scheelite-type tetragonal structure without the presence of secondary phases, in agreement with the respective Joint Committee on Powder Diffraction Standards (JCPDS) card no 44-1486. Moreover, the relative intensities and sharp diffraction of all peaks indicated that the materials are well crystallized, suggesting an ordered structure at long range. To deeply investigate the small differences in the structure of materials, the lattice parameters, the unit cell volume, and crystallite size of materials were calculated using the equation of plane spacing for the tetragonal structure and Bragg's law for diffraction. The results obtained are shown in Table 1.

Observe the values shown in Table 1 that small variations in the lattice parameters and unit cell volume indicate small lattice distortions in the $PbMoO_4$ due to the process of dissolution and recrystallization of particles occurred in the sonochemical process.

### FEG-SEM analyses of $PbMoO_4$ crystals

From FEG-SEM micrographs, it is possible to follow the evolution and growth mechanism of the $PbMoO_4$ crystal according to its synthesis time and operated amplitude. Figure 2 shows the FEG-SEM image of $PbMoO_4$ crystals obtained by co-precipitation method at room temperature without the assistance of ultrasound. It is observed in Fig. 2 that the crystals have variable morphology, some with certain roundness, others with an elongated aspect rod type. It is reasonable to state that the presence of surface defects in the $PbMoO_4$ crystal structure is associated with rapid hydrolysis during the addition of $NH_4OH$ in [27] solution. Cameirão [28] assure that the solution concentration (supersaturation) is a major factor in determining the structure of molybdates. These crystals have a primary level of agglomeration. The structure is composed of small crystals, a few nanometers in size. The growth rate of each crystal face is related to the supersaturation of the solution but nonlinearly according to Ref. [29]. The crystal growth takes place in a fast and disorderly manner,

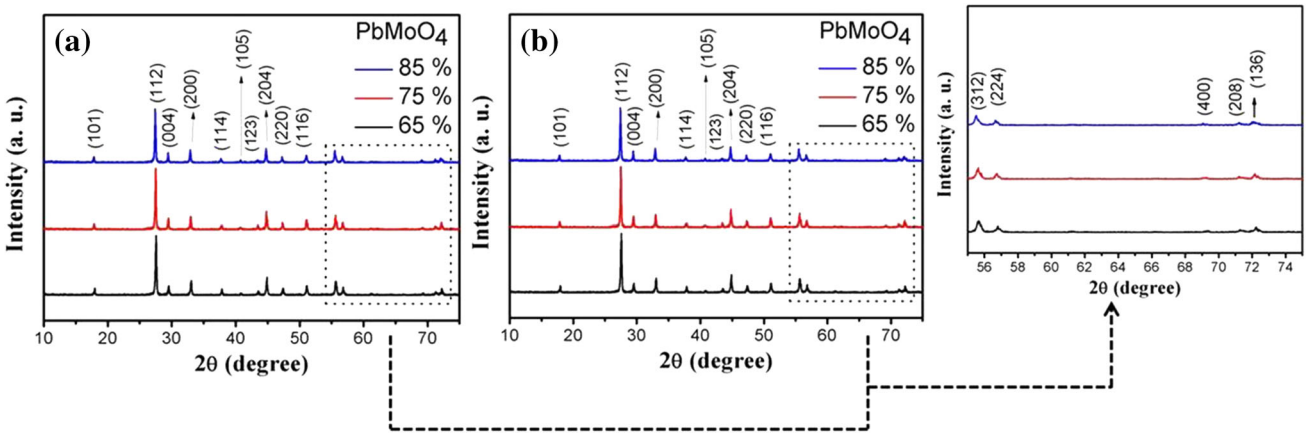


**Fig. 1** XRD patterns of $PbMoO_4$ particles processed in sonochemical method at different times (**a** 30, **b** 45 min) and amplitude (65, 75, 85%).

**Table 1** Lattice parameters, unit cell volume, and crystallite size of $PbMoO_4$ obtained in this work

| Samples (synthesis conditions) | Lattice parameters (Å) ($a = b$, $c$) | | Unit cell volume $(Å)^3$ | Crystallite size (nm) |
|---|---|---|---|---|
| 30 min—65% | 5.498 | 12.165 | 367.812 | 57.3773 |
| 30 min—75% | 5.501 | 12.169 | 368.280 | 51.6556 |
| 30 min—85% | 5.492 | 12.153 | 366.623 | 53.6438 |
| 45 min—65% | 5.483 | 12.143 | 365.186 | 56.3632 |
| 45 min—75% | 5.495 | 12.155 | 367.168 | 52.1870 |
| 45 min—85% | 5.502 | 12.174 | 368.667 | 53.0529 |
| JCPDS 44-1486 | 5.433 | 12.110 | 357.456 | – |

and within these conditions a regular morphology of the crystals cannot be obtained due to a nonlinear growth. A careful observation of the inset in Fig. 2 shows a high-magnification FEG-SEM micrograph of an individual polyhedral crystal, which indicates that the crystal is in the shape of regular 18-facet polyhedron with well-defined faces along the different crystallographic planes. According to the literature [9], the 18-facet polyhedron exhibits two {0 0 1} faces, eight {1 0 1} faces, and eight {1 1 1} faces. Figure 2b shows the average particle size distribution of $PbMoO_4$ particles processed in the co-precipitation method. It is observed that the particles have a significant variation in their sizes. The average particle value ($X_c$) is estimated at 0.4496 μm.

Figure 3 shows FEG-SEM micrographs of particles obtained in $PbMoO_4$ at different times and amplitudes by sonochemistry method. It was observed that aggregations of crystals oriented along a crystallographic direction. The micro-octahedral and the $PbMoO_4$ are interconnected through a crystallographic orientation. This morphology is achieved through an initial growth process in which adjacent crystals are self-organized in a similar crystallographic orientation (oriented attachment growth) [30], and the subsequent step is equivalent to the coalescence process. Studies of the morphology of the materials with the scheelite-type structure reported in the literature [31] observed the same mechanism growth process of oriented crystals. It is reasonable to believe that this behavior is associated with the covalent character of the Pb–O bond, and this type of chemical bond is characterized as directional. As a consequence of these bonding processes, the morphologies of materials with scheelite-type structure composed of $Pb^{2+}$ ions tend to be facetted and aligned by "docking" processes involving crystallographic fusion between some faces with high surface energy, creating an extended morphology [32].

## Average size distribution of $PbMoO_4$ crystals

Figure 4 shows the average particle size distribution of $PbMoO_4$ particles processed in the sonochemistry method at different synthesis times and amplitudes.

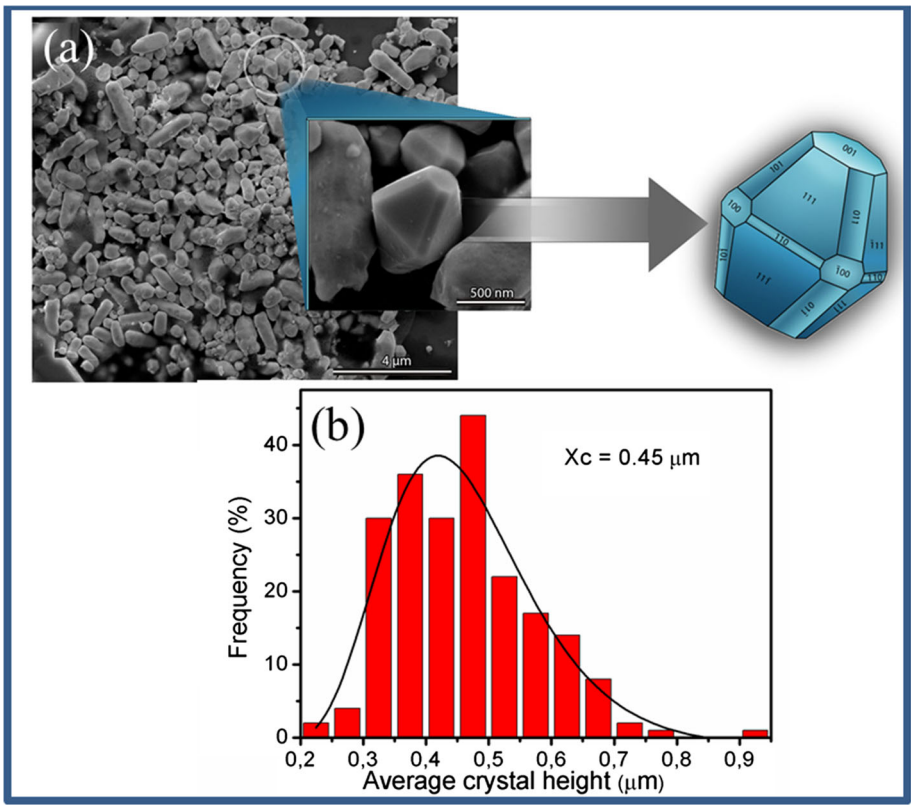


**Fig. 2** FEG-SEM micrographs of $PbMoO_4$ particles processed by the co-precipitation method.

The distribution of particle sizes observed for $PbMoO_4$ as shown in Fig. 4 is greatly influenced by the time of exposure to ultrasound and the amplitude employed in the process. There is a reduction in the average particle size of the particles due to the increase in the amplitude range of 65–75% as shown in Fig. 4a–d. This reduction is related to the acoustic cavitation phenomenon, which occurs during the ultrasonic irradiation process. The shock waves created accelerate the solid particles at high speeds, and these particles collide with each other, which can induce the fragmentation of particles. $PbMoO_4$ particles treated by a sonochemical amplitude of 65% in 30 and 45 min showed a broad-range size distribution. Almost 34% of the particles synthesized at the 30 min time are between 0.7 and 0.9 μm. For particles produced in 45 min, 28% of them correspond to the size of 0.7 μm. With the increase of the amplitude, 75% of the particles had an average reduction in their sizes according to the following values: it is estimated that 37% of the particles are in the range between 0.5 and 0.7 μm for synthesis in 30 min and 58% of particles are in the range between 0.3 and 0.5 μm for synthesis in 45 min.

In a second step using an amplitude of 85%, it is observed that the particles had an increase in their average sizes. This behavior has been discussed by Suslick and Price [33], who suggest that the propagation of shock waves may induce the sintering of solid particles of the solute in a liquid–solid system, from collisions between particles at straight angles.

An estimated 48% of the particles produced under the conditions of 85% amplitude and 30 min are in the range of 1–1.4 μm. About 50% of the particles produced in 45 min are in the range of 1.25–1.75 μm. There was a significant increase in the size due to coalescence of particles during the sintering process. Cavitations and shock waves created by ultrasound can accelerate solid particles to high velocities, leading to interparticle collisions and inducing an effective fusion at the point of collision.

## Growth mechanism of $PbMoO_4$ crystals

Figure 5 shows the schematic representation of the main growth mechanisms involved in the synthesis of $PbMoO_4$ crystals by the sonochemical method. The crystal growth is controlled by extrinsic and intrinsic

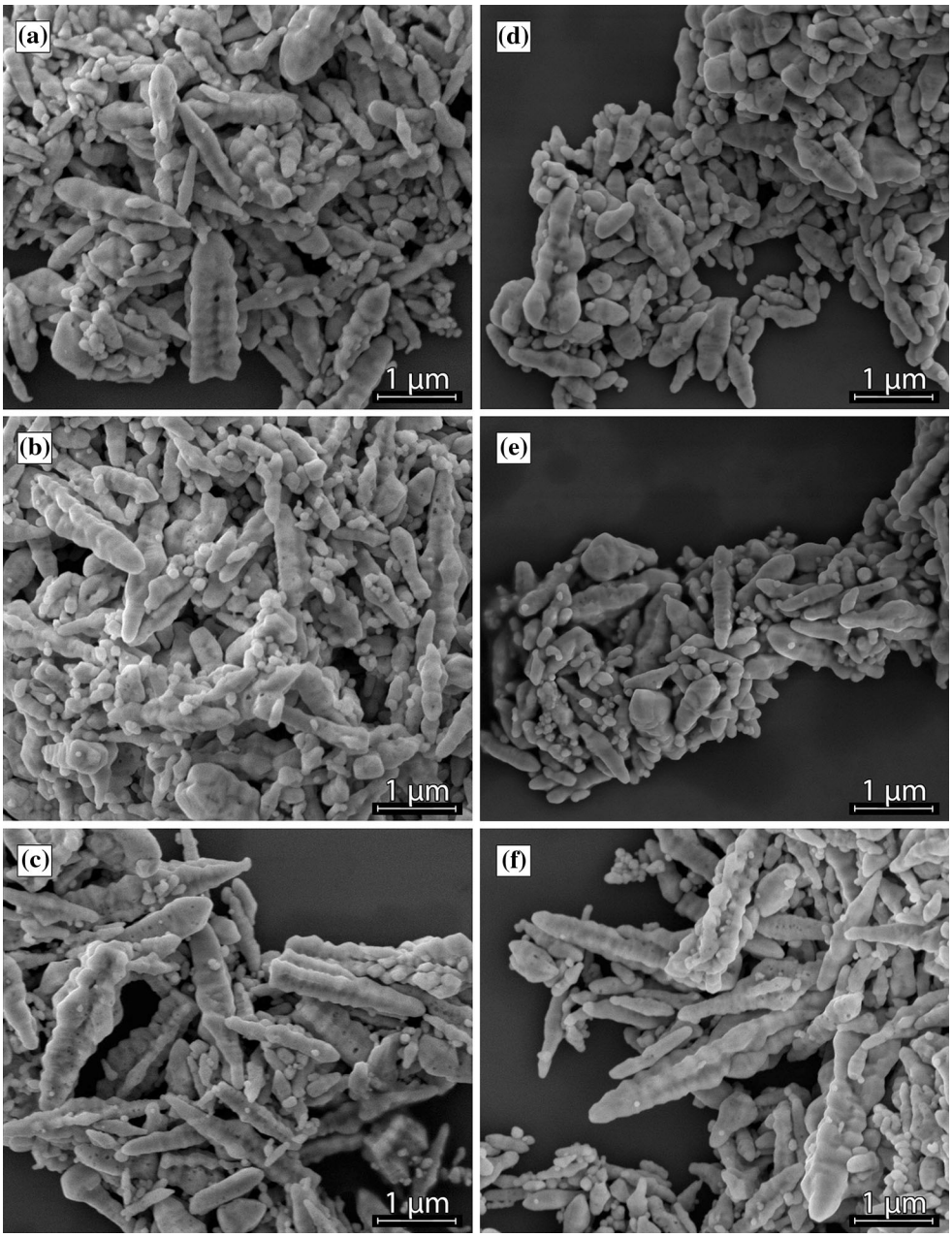


**Fig. 3** FEG-SEM micrographs of $PbMoO_4$ particles processed by the sonochemical method—**a** 65%, **b** 75%, and **c** 85% amplitude in 30 min; **d** 65%, **e** 75%, and **f** 85% amplitude in 45 min.

factors, including the degree of supersaturation, diffusion of the reaction, surface energy, crystal structure, and solution parameters. Several well-known crystal growth mechanisms in the solution system are the oriented attachment and Ostwald ripening process. The formation of small octahedral $PbMoO_4$ occurred from the dissolution of the precursors [$H_2MoO_4$ and $Pb(NO_3)_2$] in deionized water. This solution is a fast ionization and dissociation acid salt, and the ions of $Pb^{2+}$ and $(MoO_4)^{2-}$ are instantly solvated by $H_2O$ molecules. The difference in the electron density between $Pb^{2+}$ and $(MoO_4)^{2-}$ ions promotes the electrostatic attraction between them resulting in the precipitation/crystallization process (Fig. 5a). The increase in the precipitation rate is observed with the addition of $NH_4OH$ solution to generating a disordered growth of the crystals due to a rapid process of self-assembly during the precipitation material. When the $PbMoO_4$ crystals are exposed to the irradiation of ultrasound, the energy

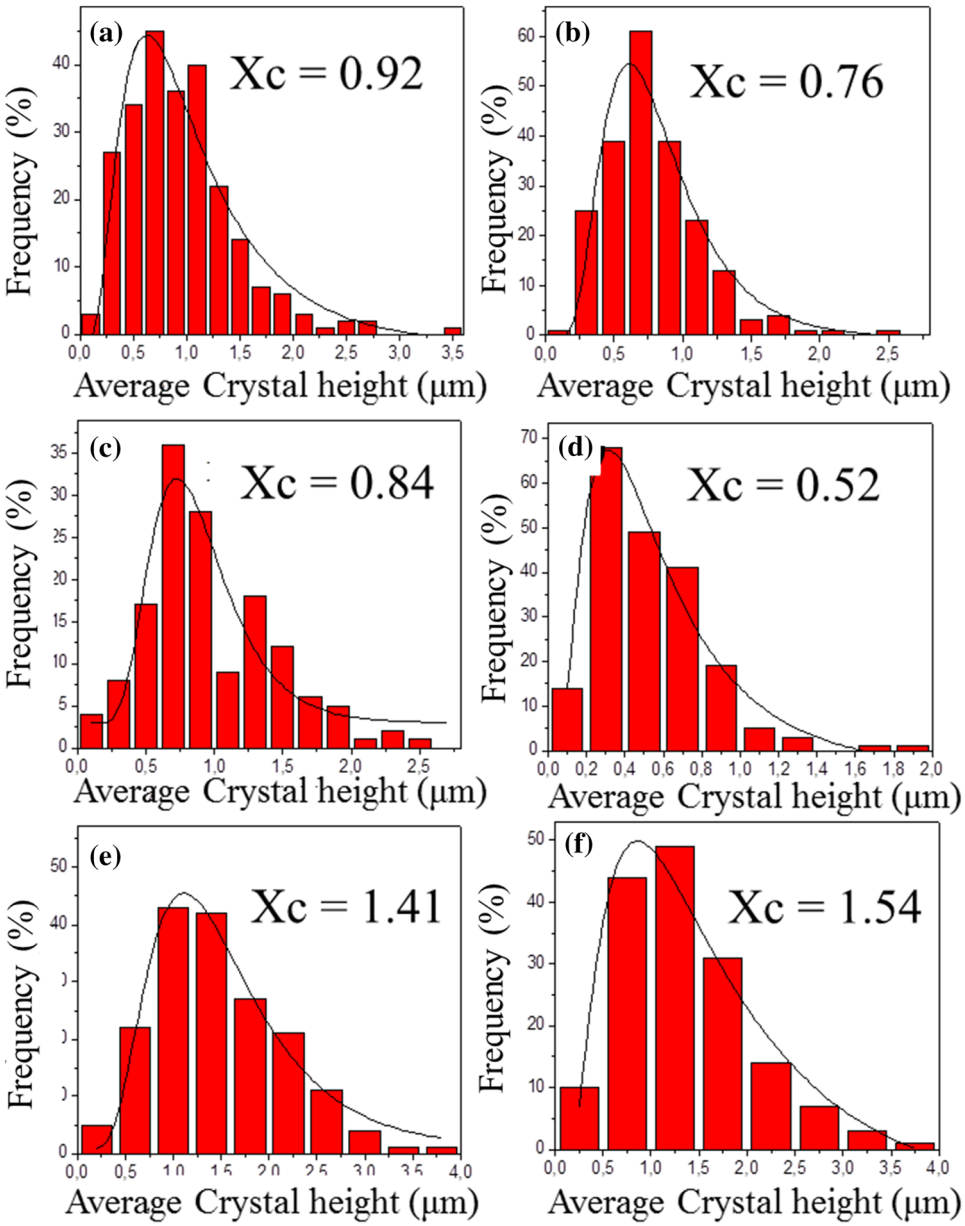


**Fig. 4** Average particle size distribution of $PbMoO_4$ particles processed by the sonochemical method at **a** 65%—30 min, **b** 65%—45 min, **c** 75%—30 min, **d** 75%—45 min, **e** 85%—30 min, and **f** 85%—45 min.

supplied to the solution allows the dissolved crystals to start a recrystallization process (Fig. 5b), which is attributed to the cavitational effects resulting out of the high frequency irradiation. The crystals obtained at this stage obtained significant growth and an average size of 1.35 μm. Subsequently, $PbMoO_4$ particles have an anisotropic growth and formation of irregular micro-octahedrons. This growth mechanism is known as Ostwald Ripening, where small particles are less thermodynamically stable than larger ones. This coalescence occurs which promotes growth (Fig. 5c). The average particle size of this step is around 1.73 μm. The $PbMoO_4$ crystals show a growth model oriented in the crystallographic direction [001]. This type of crystal growth mechanism is called the Oriented Attachment. Figure 5d shows the particles with dendritic structure. There is a main trunk and four cross arms extending from the center of the main trunk. Crossed branches build the structure of a perfect perpendicular. It is observed that the dendritic morphology is formed by nanopolyhedrons arranged which are connected to each other in an interesting way. This type of morphology is described in previous work [34, 35].

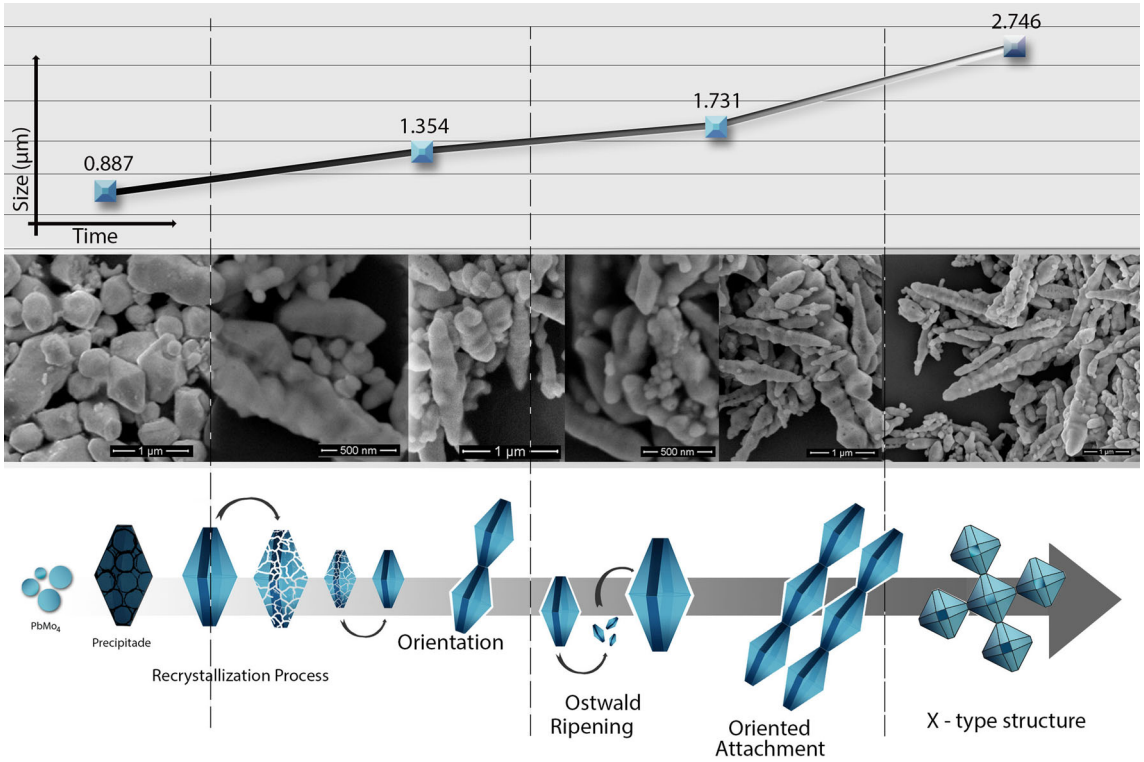


**Fig. 5** A schematic illustration of the growth mechanism of $PbMoO_4$ crystals by the sonochemical method.

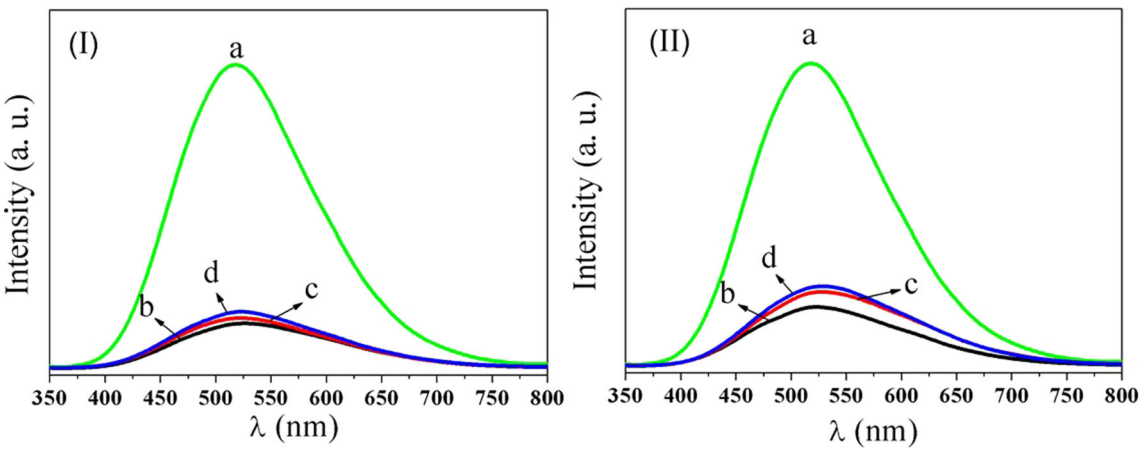


**Fig. 6** Photoluminescence spectra of $PbMoO_4$ crystals (I) 30 and (II) 45 min: *a* co-precipitation, *b* 65%, *c* 75%, and *d* 85% amplitude.

In order to provide evidence that growth of $PbMoO_4$ particles is through an oriented mechanism, as suggested in the model of Fig. 5, TEM measurements were performed to evidence the oriented attachment growth of the $PbMoO_4$ particles in our study. It is shown in Fig. SI 1 of the support information section.

## Photoluminescence characteristics of $PbMoO_4$ crystals

Figure 6 shows the PL spectra of the $PbMoO_4$ samples synthesized by co-precipitation method and the samples that received the sonochemical treatment at different amplitudes and synthesis times, which were

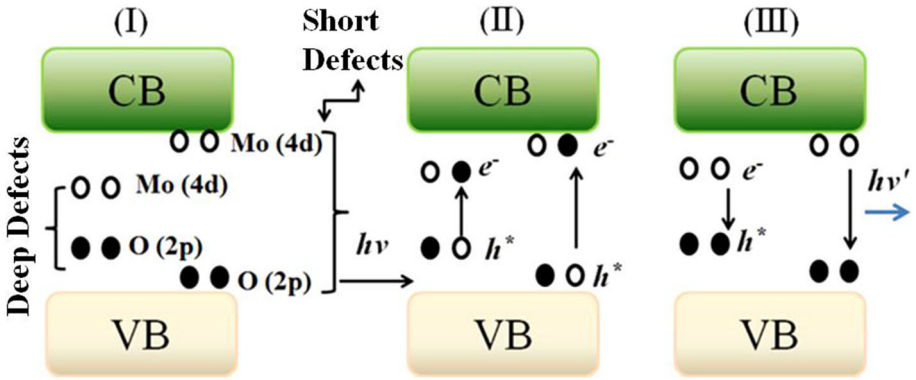


**Fig. 7** Model proposed to explain the photoluminescence of $PbMoO_4$.

investigated at an excitation wavelength of 350 nm and measured from 350 to 800 nm. High emission intensity for the $PbMoO_4$ obtained by co-precipitation method is observed. It is suggested that this behavior is associated with the particle morphology as presented in Fig. 2. The micrographs indicated that the crystals produced by the co-precipitation method present a smaller average particle size, i.e., because of the nucleation rate, the instant that $Pb^{2+}$ and $MoO_4^{2-}$ ions are dissolved in the solution is higher than the growth rate of the crystals. The difference in the electron density among these ions promotes an intense electrostatic force favoring the appearance of small crystals. Samples treated with sonochemical method had a low PL emission intensity. This result is combined with the morphologic characteristics described in Fig. 3. The effect of high energy released by the cavitation phenomenon in ultrasonic processing conditions promotes the $PbMoO_4$ crystal growth, resulting in particles with larger sizes, a higher degree of agglomeration and an array of orientation in the crystal growth. It is proposed that these aspects could interfere with photoluminescent properties. Yang [36] attributed the origin of the PL properties to the morphology, degree of crystallinity, and particle sizes.

These results indicate that the PL intensity depends strongly on the morphology and crystallinity of the crystals. The spectrum shows that the sample has a typical green emission peak at about 525 nm. The emission spectrum of the metal molybdates might be ascribed to the charge-transfer transitions within the $[MoO_4]$ clusters [37]. During the excitation process at room temperature, the electrons situated at lower intermediary energy levels (oxygen 2p states) absorb the photon energy arising from 350 nm (3.54 eV) wavelength. As a consequence of this phenomenon, the energetic electrons are promoted to higher intermediary energy levels (molybdenum 4d states) located near the conduction band. When the electrons fall back to lower energy states again via radiative return processes, the energy arising from this electronic transition is converted into photons. In this case, the several photons originated by the participation of different energy states during the electronic transitions are responsible for the broad PL spectra.

In Fig. 7 is shown a proposed model which explains the behavior of the micro-octahedron $PbMoO_4$ luminescence by a random distortion of both $[MoO_4]$ and $[PbO_8]$ clusters.

(1) The presence of intermediate energy levels, represented by short and deep defects within the material gap, is observed.
(2) Electron transition of oxygen 2p orbitals in the valence band (VB) for molybdenum 4d orbitals by absorption of ($h\upsilon$) to conduction band (CB).
(3) Photon emission process ($h\upsilon'$) due to the radiative return of the electrons located in the 4d orbitals to the 2p orbitals of the oxygen.

Small magnitude distortions in the $[MoO_4]$ clusters are responsible for promoting a slight deformation in the bonds Pb–O. These distortions are capable of inducing a symmetry in the crystalline lattice, leading to the appearance of intermediate levels within the band gap of the $PbMoO_4$ crystals and a gradient of charge between the clusters [29]. These intermediate levels facilitate the electronic transitions in the band gap.

The color coordinates were calculated for all $PbMoO_4$ samples using CIE 1931 color matching functions. Figure 8 shows CIE 1931 chromaticity diagram of the investigated $PbMoO_4$ powders. It is observed that most color coordinate values fell in the green color region. The $x$ and $y$ values are shown in Table 2.

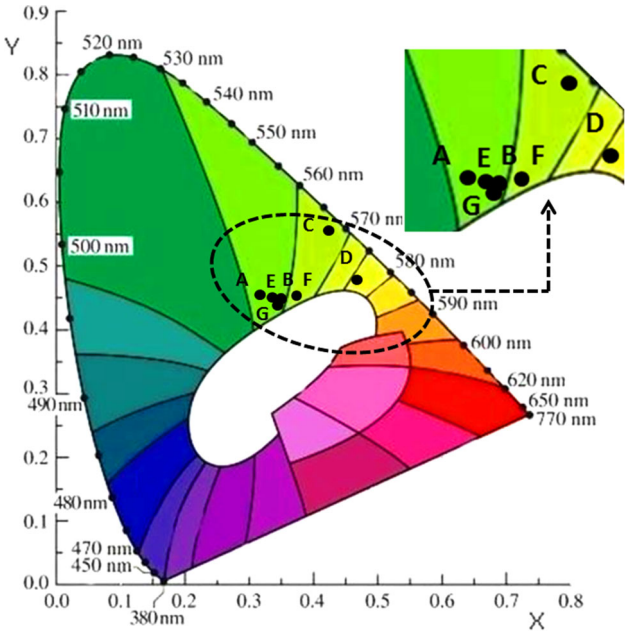


**Fig. 8** CIE diagram of $PbMoO_4$ particles.

## UV–Visible absorption spectroscopy

The energy band (*E*gap) $PbMoO_4$ of particles was calculated using the Kubelka–Munk method [38], which consists in converting diffuse reflectance measurements in $E_{gap}$ values. The Kubelka–Munk relationship is described in Eq. 1:

$$F(R\infty) = \frac{k}{s} = \frac{(1 - R\infty)^2}{2R\infty}, \quad (1)$$

where $F(R)$ is the Kubelka–Munk function. In this study, the standard sample used for the analysis was the $BaSO_4$. $R\infty = R(PbMoO_4)/R(BaSO_4)$, ($R\infty$ is the percentage of reflected light), $k$ is the molar absorption coefficient, and $s$ is the scattering coefficient.

The energy gap semiconductor oxides can be calculated by Eq. 2:

$$\alpha hv = C_1(hv - E_{gap})^n, \quad (2)$$

where $\alpha$ is the linear absorption coefficient, $hv$ is the photon energy, $C_1$ is a proportionality constant, $E_{gap}$ is the optical gap, and $n$ is a constant related to different types of electronic transitions ($n = 1/2$ for a direct allowed, $n = 2$ for an indirect allowed). According to the literature, the molybdate materials exhibit an optical absorption spectrum governed by direct electronic transitions [39]. Figure 9 represents the band gap determination graph of the samples by extrapolating the line.

The gap energy obtained for $PbMoO_4$ samples showed a small difference in values between the range of 3.03 and 3.23 eV. This behavior is due to the intermediate energy levels within the band gap. The appearing of these levels is associated with the degree of structural order–disorder in the material lattice. The increase in structural organization promotes the decrease in the number of intermediate levels, and in view of this the energy gap shows higher values [40]. Other factors may also justify that the difference found in the $E_{gap}$ could be related to synthesis conditions (processing temperature and time), the shape of the materials (film or powder), and the chemical method to obtain the material. Other experimental aspects such as the preparation of the material, as well as the morphology of the particles, can influence the gap energy.

## Conclusions

$PbMoO_4$ was successfully synthesized using the sonochemical method with different synthesis times and amplitudes. XRD observation revealed the good crystallinity of the prepared samples without any associated impurities. Increasing the ultrasonic amplitude from 65 to 75% resulted in a decrease in the average size of the $PbMoO_4$ particles due to crushing effect of high cavitation energy. In a second stage, it was observed that the

**Table 2** The chromaticity coordinates for $PbMoO_4$ particles

| Conditions of synthesis (time/amplitude) | Code | Coordinate (*x*, *y*) | Color |
|---|---|---|---|
| Co-precipitation | A | 0.32, 0.45 | Yellowish green |
| 30 min/65% | B | 0.35, 0.44 | Yellowish green |
| 30 min/75% | C | 0.43, 0.56 | Yellow green |
| 30 min/85% | D | 0.47, 0.48 | Yellow |
| 45 min/65% | E | 0.34, 0.45 | Yellowish green |
| 45 min/75% | F | 0.36, 0.45 | Yellow green |
| 45 min/85% | G | 0.35, 0.45 | Yellowish green |

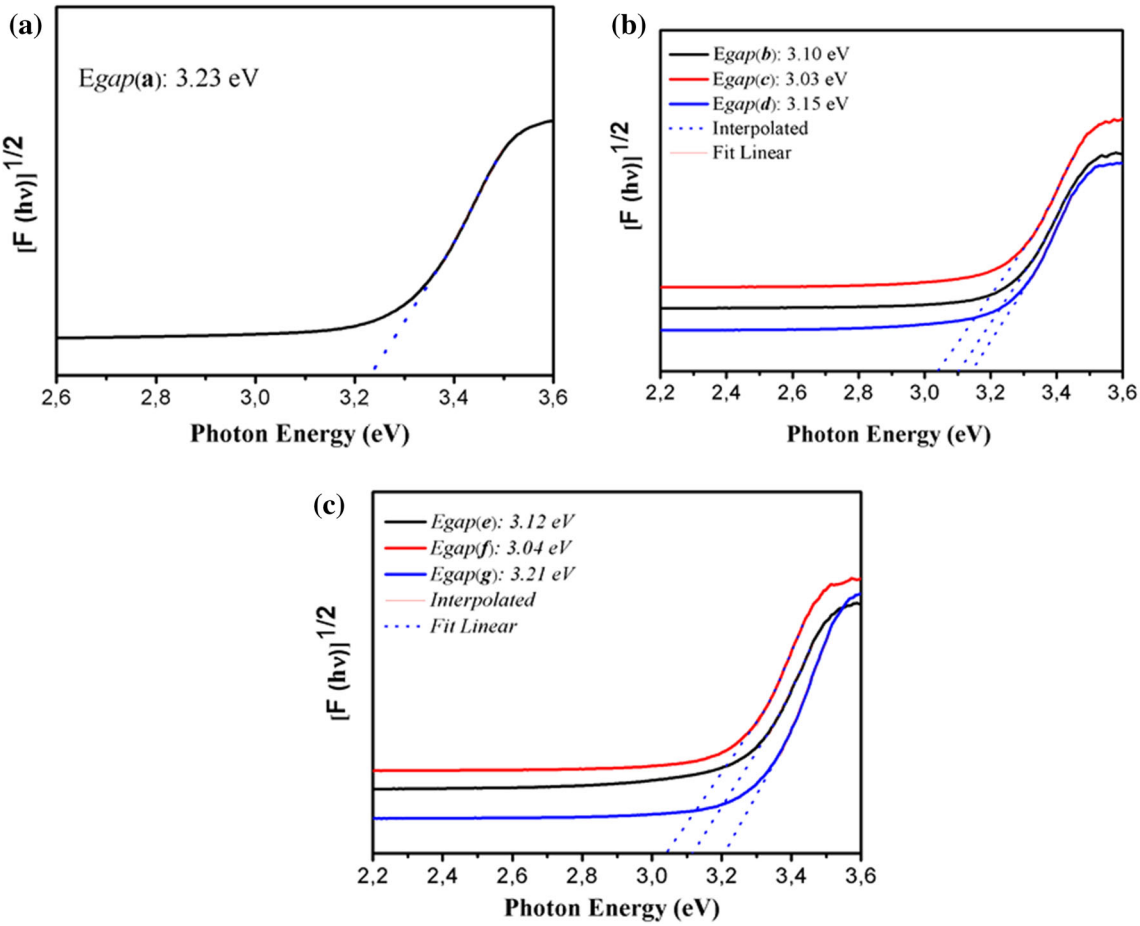


**Fig. 9** Determination of the gap by Kubelka–Munk method for particles synthesized at different times: **a** co-precipitation method, **b** 30 min/65%, **c** 30 min/75%, **d** 30 min/85%, **e** 45 min/65%, **f** 45 min/75%, **g** 45 min/85%.

average particle size increases when an amplitude of 85% is employed to it. This increase can be related to the particle coalescence process between PbMoO4 particles due to the high temperatures produced by sonochemical method, thereby favoring the sintering process of $PbMoO_4$ particles.

From the study of crystal growth, it was considered an evolution in the $PbMoO_4$ particle morphology as a function of exposure time to ultrasound in the sample. Initially, precipitates are obtained from a disordered crystal growth. After a short synthesis time, there is a preferential orientation along [001] in crystals by an Oriented Attachment mechanism. For longer synthesis time, note that the crystals exhibit new preferred growth directions. In the latter case, the morphology of the particles has a dendritic structure. The behavior of the PL has been associated with charge-transfer-type transitions within the $[MoO_4]$ clusters. Just as the existence of structural defects is causing photon emission, the synthesis conditions strongly influence the morphology and the average particle size as a result of which the photoluminescent properties were also affected. The change in the values found for the energy gap from the UV–Vis analysis absorption spectra are justified by the presence of intermediate energy levels [O (2p) and Mo (4d)] within the gap. The values of Gap are in the range of 3.03 and 3.23 eV.

## Acknowledgement

We dedicate in particular the present article to O. L. A. Conceição, who is no longer among us, but who left us a cooperation of great value for the accomplishment in this work. The authors gratefully acknowledge the financial support of the Brazilian governmental research funding agencies CAPES, CNPq 402127/2013-7, FAPESP, and INCTMN.

**Electronic supplementary material:** The online version of this article (doi:10.1007/s10853-016-0705-y) contains supplementary material, which is available to authorized users.

## References


[1] Araújo VD, Tranquilin RL, Motta FV, Paskocimas CA, Bernardi MIB, Cavalcante LS, Andres J, Longo E, Bomio MRD (2014) Effect of polyvinyl alcohol on the shape, photoluminescence and photocatalytic properties of $PbMoO_4$ microcrystals. Mater Sci Semicond Process 26:425–430

[2] Zhiyong Y, Chaonan D, Ruiying Q, Lijin X, Aihua Z (2015) Photocatalytic degradation of methyl orange by $PbXO_4$ (X = Mo, W). J Colloid Interface Sci 438:323–331

[3] Danevich FA et al (2010) Feasibility study of $PbWO_4$ and $PbMoO_4$ crystal scintillators for cryogenic rare events experiments. Nucl Instrum Methods Phys Res A 622:608–613

[4] Guo C, Xu J, Wang S, Li L, Zhang Y, Li X (2012) Facile synthesis and photocatalytic application of hierarchical mesoporous $Bi_2MoO_6$ nanosheet-based microspheres. Cryst Eng Comm 14:3602–3608

[5] Duan FZ, Yan C, Ming Q (2011) Enhanced photocatalytic activity of bismuth molybdate via hybridization with carbon. Mater Lett 65:191–193

[6] Wang L, Tang H, Tian Y (2016) Carbon-shell-decorated p-semiconductor $PbMoO_4$ nanocrystals for efficient and stable photocathode of photoelectrochemical water reduction. J Power Sources 319:210–218

[7] Skibiński T, Kaczmarek SM, Leniec G, Tsuboi T, Nakai Y, Berkowski M, Kowalski Z, Huang W (2014) Magnetic and optical properties of Co-doped $PbMoO_4$ single crystals. J Cryst Growth 401:802–806

[8] Hernández-Uresti DB, Martínez-de la Cruz A, Aguilar-Garib JA (2013) Photocatalytic activity of $PbMoO_4$ molybdate synthesized by microwave method. Catal Today 212:70–74

[9] Sczancoski JC, Bomio MDR, Cavalcante LS, Joya MR, Pizani PS, Varela JA, Longo E, Li MS, Andrés JA (2009) Morphology and blue photoluminescence emission of $PbMoO_4$ processed in conventional hydrothermal. J Phys Chem C 113:5812

[10] Dong FQ, Wu QS (2008) Synthesis of homogeneous bunched lead molybdate nanobelts in large scale via vertical SLM system at room temperature. Appl Phys A Mater Sci Process 91:161

[11] Jia S, Zheng H, Sang H, Zhang W, Zhang H, Liao L, Wang J (2013) Self-assembly of $K_xWO_3$ nanowires into nanosheets by an oriented attachment mechanism. ACS Appl Mater Interfaces 5:10346–10351

[12] Hernández-Urestia DB, Martínez-de la Cruz A, Torres-Martínez LM (2016) Photocatalytic degradation of organic compounds by $PbMoO_4$ synthesized by a microwave-assisted solvothermal method. Ceram Int 42:3096–3103

[13] De Yoreo JJ, Vekilov P (2003) Principles of crystal nucleation and growth, Chapter 3. In: Dove PM (ed) Biomineralization. Mineralogical Society of America, Washington, p 57

[14] Cavalcante LS, Sczancokis JC, Tranquilin RL, Varela JA, Longo E, Orlandi MO (2009) Growth mechanism of octahedron-like $BaMoO_4$ microcrystals processed in microwave-hydrothermal: experimental observations and computational modeling. Particuology 7:353–362

[15] Bordui P (1987) Growth of large single crystals from aqueous solution: a review. J Cryst Growth 85:199

[16] Cui C et al (2007) Unique photoluminescence properties of highly crystallized $BaMoO_4$ film prepared by chemical reaction. Mater Lett 61:4525–4527

[17] Zhang Y et al (2005) Synthesis of crystalline $SrMoO_4$ nanowires from polyoxometalates. Solid State Commun 133:759–763

[18] Zhang G et al (2006) Preparation, structural and optical properties of $AWO_4$ (A = Ca, Ba, Sr) nanofilms. Mater Sci Eng, B 128:254–259

[19] Errandonea D, Manjón FJ (2008) Pressure effects on the structural and electronic properties of $ABX_4$ scintillating crystals. Prog Mater Sci 53:711–773

[20] Tyagi M et al (2008) New observations on the luminescence of lead molybdate crystals. J Lumin 128:22–26

[21] Piwowarska D, Kaczmarek SM, Berkowski M (2008) Dielectric, optical and EPR studies of PbMoO4 single crystals pure and doped with cobalt ions. J Non-Cryst Solids 354:4437–4442

[22] Sangeeta DG et al (2006) Non-stoichiometry-induced cracking in $PbMoO_4$ crystals. J Cryst Growth 296:81–85

[23] Yang L, Wang Y, Wang X, Han G (2013) Synthesis of $PbMoO_4$ nanorods by a simple sonochemical method. J Ceram Soc Jpn 121:745–748

[24] Bhanvase BA, Darda NS, Veerkar NC, Shende AS, Satpute SR, Sonawane SH (2015) Ultrasound assisted synthesis of PANI/$ZnMoO_4$ nanocomposite for simultaneous improvement in anticorrosion, physico-chemical properties and its application in gas sensing. Ultrason Sonochem 24:87–97

[25] Seeharaja P, Boonchomb B, Charoonsukc P, Kim-Lohsoontornd P, Vittayakorna N (2013) Barium zirconate titanate nanoparticles synthesized by the sonochemical method. Ceram Int 39:S559–S562

[26] Zhang J, Li L, Zi W, Guo N, Zou L, Gan S, Ji G (2014) Self-assembled $CaMoO_4$ and $CaMoO_4$: $Eu^{3+}$ hierarchical superstructures: Facile sonochemical route synthesis and tunable luminescent properties. J Phys Chem Solids 75:878–887

[27] Marques VS, Cavalcante LS, Sczancoski JC, Alcântara AFP, Orlandi MO, Moraes E, Longo E, Varela JA, Siu Li M, Santos MRMC (2010) Effect of different solvent ratios (water/ethylene glycol) on the growth process of $CaMoO_4$ crystals and their optical properties. Cryst Growth Des 10:4752

[28] Cameirão A, David R, Espitalier F, Gruy F (2008) Effect of precipitation conditions on the morphology of strontium molybdate agglomerates. J Cryst Growth 310:4152–4162

[29] Bomio MRD, Cavalcante LS, Almeida MAP, Tranquilin RL, Batista NC, Pizani PS, Siu Li M, Andres E, Longo E (2013) Structural refinement, growth mechanism, infrared/Raman spectroscopies and photoluminescence properties of $PbMoO_4$ crystals. Polyhedron 50:532–545

[30] Penn RL, Banfield JF (1998) Imperfect oriented attachment: dislocation generation in defect-free nanocrystals. Science 281:969–971

[31] Yang F, Liu Y, Lu Y, Chen H, Zhang D, Wu H (2014) Morphology and photoluminescence properties of $KSm(MoO_4)_2$ microcrystals by a molten salt method. J Mater Sci 25:3608–3613

[32] Colfen H, Mann S (2003) Higher-order organization by mesoscale self-assembly and transformation of hybrid nanostructures. Angew Chem Int Ed 42:2350

[33] Suslick KS, Price GJ (1999) Applications of ultrasound to materials chemistry. Annu Rev Mater Sci 29:295–326

[34] Tian Y et al (2012) Ionic liquid-assisted hydrothermal synthesis of dendrite-like $NaY(MoO_4)_2$:$Tb^{3+}$ phosphor. Phys B 407:2556–2559

[35] Cheng Y, Wang Y, Chen D, Bao F (2005) Evolution of single crystalline dendrites from nanoparticles through oriented attachment. J Phys Chem B 109:794–798

[36] Yang J, Lu C, Su H, Ma J, Cheng H, Qi L (2008) Morphological and structural modulation of $PbWO_4$ crystals directed by dextrans. Nanotechnology 19:035608

[37] Sczancoski JC, Cavalcante LS, Marana NL, Silva RO, Tranquilin RL, Joya MR, Pizani PS, Varela JA, Sambrano JR, Li MS, Longo E, Andrés J (2010) Electronic structure and optical properties of $BaMoO_4$ powders. Curr Appl Phys 10:614–624

[38] Kubelka P, Munk F (1931) Ein Beitrag Zur Optik der Farbanstriche. Z fur tech Phys 12:593–601

[39] Cavalcante LS et al (2013) A combined theoretical and experimental study of electronic structure and optical properties of β-$ZnMoO_4$ microcrystals. Polyhedron 54:13–25

[40] Efendiev S, Darvishov N, Shakhdgan S, Gavryushin V, Raciukaitis G, Puzonas G, Kazlauskas A (2006) Two-phonon spectroscopy of $PbMoO_4$ single crystals. Phys Status Solidi B 156:697